

# Bifunctional Passivation through Fluoride Treatment for Highly Efficient and Stable Perovskite Solar Cells

Chang Liu, Jiyao Zhang, Luozheng Zhang, Xianyong Zhou, Yanliang Liu, Xingzhu Wang,\* and Baomin Xu\*

Due to the low formation energy, surface defects are more likely to form on the surface of  $\text{TiO}_2$  films, resulting in a decline in the efficiency and stability of perovskite solar cells (PSCs). Additionally, defects on the bottom surface of the perovskite layer in contact with  $\text{TiO}_2$  play a key role in  $V_{oc}$  (open circuit voltage) loss and the PSC degradation process. Therefore, to improve the efficiency and stability of PSCs, it is critical to develop a reproducible and low-cost method for passivating the defects on both the  $\text{TiO}_2$  surface and on the bottom surface of the perovskite layer. In this work, fluoride is utilized as a bifacial contact passivation agent for decreasing the number of defects on the  $\text{TiO}_2$  surface and the bottom surface of the perovskite layer. PSC efficiency can be significantly increased from 21.3% to 23.7% with fluoride passivation. In addition, the long-term stability of PSCs, especially light irradiation stability, can be markedly improved. The passivation effects of fluoride treatment on  $\text{TiO}_2$  films are studied by theoretical calculation and experimental characterization. This work provides a thorough understanding of the  $\text{TiO}_2$ /perovskite interface and demonstrates an approach for improving the efficiency and stability of PSCs.

by providing charge transport channels.<sup>[9,10]</sup> Two major factors contribute to the high performance of m- $\text{TiO}_2$ -based PSCs. One factor is the excellent properties of  $\text{TiO}_2$ , such as low optical losses, high electron mobility, high transmittance, and a matched energy level with perovskite materials.<sup>[11]</sup> The other factor is the mesoporous structure of  $\text{TiO}_2$ , which can provide a more stable growth template for perovskite and a larger contact area to facilitate electron transport between the perovskite and the  $\text{TiO}_2$  layer.<sup>[12]</sup> Consequently, devices with an m- $\text{TiO}_2$  ETL have excellent PSC performance.

Although the m- $\text{TiO}_2$  ETL has clear advantages, the m- $\text{TiO}_2$  layer still has a serious drawback. Hydroxyl groups are usually absorbed on the  $\text{TiO}_2$  surface, resulting in trap states in the valence band of  $\text{TiO}_2$ .<sup>[13]</sup> These defect sites on the  $\text{TiO}_2$  surface will be one of the factors causing nonradiative recombination at the inter-

## 1. Introduction

In recent years, perovskite solar cells (PSCs) have become a popular topic of research spots due to their rapidly increasing efficiency and low fabrication cost.<sup>[1–3]</sup> Many types of PSCs have been developed, including mesoporous structures, regular structures, and inverted structures.<sup>[4–6]</sup> Among them, mesoporous structure-based PSCs have achieved high efficiency and attracted much attention.<sup>[7,8]</sup> In the mesoporous structure, the mesoporous titanium oxide (m- $\text{TiO}_2$ ) electron transport layer (ETL) contributes to PSC efficiency and stability


face between the  $\text{TiO}_2$  and perovskite, potentially reducing the efficiency of the PSC device. Additionally, under light irradiation, the hydroxyl groups can trap the photogenerated charges from the  $\text{TiO}_2$  and form highly oxidizing superoxide radicals, leading to the decomposition of the perovskite layer.<sup>[14]</sup> In addition to the defects on the  $\text{TiO}_2$  surface, defects on the bottom surface of the perovskite layer, at the interface between the  $\text{TiO}_2$  layer and the perovskite, also play a crucial role in PSC efficiency.<sup>[15,16]</sup> Previous theoretical and experimental studies have shown that a large number of defects typically form in the perovskite layer at the interface due to lattice mismatch,

C. Liu, J. Zhang, L. Zhang, X. Wang  
Academy for Advanced Interdisciplinary Studies  
Southern University of Science and Technology  
Shenzhen 518055, China  
E-mail: wangxz@sustech.edu.cn

C. Liu, J. Zhang, L. Zhang, X. Zhou, Y. Liu, X. Wang, B. Xu  
Department of Materials Science and Engineering and Shenzhen  
Engineering Research and Development Center for Flexible Solar Cells  
Southern University of Science and Technology  
Shenzhen 518055, China  
E-mail: xu.bm@sustech.edu.cn

C. Liu, J. Zhang, L. Zhang, X. Zhou, Y. Liu, X. Wang, B. Xu  
Key University Laboratory of Highly Efficient Utilization of Solar Energy  
and Sustainable Development of Guangdong  
Southern University of Science and Technology  
Shenzhen 518055, China

C. Liu, J. Zhang, L. Zhang, X. Zhou, Y. Liu, X. Wang, B. Xu  
Guangdong-Hong Kong-Macao Joint Laboratory for  
Photonic-Thermal-Electrical Energy Materials and Devices  
Southern University of Science and Technology  
Shenzhen 518055, China

 The ORCID identification number(s) for the author(s) of this article can be found under <https://doi.org/10.1002/aenm.202200945>.

DOI: 10.1002/aenm.202200945

resulting in charge recombination and moisture permeation.<sup>[17,18]</sup> This is an important factor that contributes to a low open circuit voltage, hysteresis, and device instability. To limit the negative effect of defects on the performance of PSCs, some multifunctional materials have been developed to passivate the ionic defects at the interface.<sup>[19,20]</sup> However, most researches thus far have only focused on one kind of defect: either defects on the TiO<sub>2</sub> surface or defects on the perovskite layer. It has been demonstrated that introducing chloride ions (Cl<sup>-</sup>) on the TiO<sub>2</sub> surface is an effective method for passivating defects at the interface and improving the photovoltaic performance of PSCs.<sup>[21]</sup> Choline chloride with positively and negatively charged components has been reported to increase the carrier recombination lifetime and reduce the charge trap density, significantly improving the efficiency of PSCs.<sup>[22]</sup> For TiO<sub>2</sub>, utilizing Cl<sup>-</sup> as a modification agent can improve PSC performance due to the enhanced electronic properties of TiO<sub>2</sub>.<sup>[23]</sup> Compared with Cl<sup>-</sup>, fluorine ions (F<sup>-</sup>) with higher electronegativity may exhibit a better passivation effect due to chemical bonding enhancement. F<sup>-</sup> has also been used as a perovskite material additive to improve the efficiency and stability of PSCs.<sup>[24]</sup> In conclusion, both defects on the TiO<sub>2</sub> surface and defects on the bottom surface of the perovskite layer are significantly detrimental to PSC performance, but little research has been conducted on passivating both kinds of defects at the same time. Therefore, it remains both urgent and challenging to develop an effective strategy to simultaneously decrease the number of defects on the TiO<sub>2</sub> surface and on the bottom surface of the perovskite layer.

Here, we report an effective post-treatment strategy for reducing TiO<sub>2</sub> surface defects and passivating defects on the bottom surface of the perovskite layer by introducing bifunctional fluoride. We first fabricate state-of-the-art mesoporous TiO<sub>2</sub> and then deposit fluoride on the TiO<sub>2</sub> surface using a soaking treatment. In this work, hydrofluoric acid (HF) was used as the source of fluoride because its acidity can be beneficial for reacting with basic hydroxyls and the product H<sub>2</sub>O is easy to remove. As expected, a hydrogen cation from the HF could react with the hydroxyl groups on the TiO<sub>2</sub> surface, and fluoride anions can substitute into the defect sites, resulting in energy level tuning and improved electron extraction from the perovskite. In addition, fluoride ions on the TiO<sub>2</sub> surface form strong ionic bonds with the Pb<sup>2+</sup> ions in the perovskite lattice, effectively passivating the anionic vacancy defects in the perovskite. Perovskite films with reduced defects will effectively improve charge transfer and inhibit interfacial charge recombination. With fluoride passivation, the efficiency of PSCs can be increased significantly, from 21.3% to 23.7%. More importantly, unencapsulated fluoride-passivated devices exhibit excellent long-term stability. The PSC device can retain over 90% of its original PCE under continuous illumination for 1000 h.

## 2. Results and Discussion

As shown in **Figure 1a**, we assumed that hydroxyl groups could be removed from the TiO<sub>2</sub> surface by the HF surface treatment. Also, the TiO<sub>2</sub> surface could be doped with fluorine ions treatment. We predicted that an acidic hydrogen cation in the HF

could react with the -OH group on the TiO<sub>2</sub> surface, which forms water vapor. Subsequently, fluoride anions could substitute into the defect sites generated by the evolution of the -OH group, potentially leading to energy level tuning. We tested this theory by comparing X-ray photoelectron spectroscopy (XPS) data for a pristine TiO<sub>2</sub> surface versus an HF-treated TiO<sub>2</sub> surface (**Figure 1b,c**). The peaks belonging to the Ti 2p in XPS spectra were differed by 6.3 eV, which is in accord with the tetravalent oxidation Ti of TiO<sub>2</sub>.<sup>[25]</sup> When compared to pristine TiO<sub>2</sub>, these two peaks for the TiO<sub>2</sub> with HF treatment are downshifted 0.15 eV toward a lower binding energy. The reason for this peak shift can be attributed to the conversion of Ti<sup>4+</sup> to Ti<sup>3+</sup> by charge compensation induced by slight F-doping, which may reduce the binding energy of Ti-O-Ti. The O 1s peaks in XPS spectra for pristine TiO<sub>2</sub> and TiO<sub>2</sub> with HF treatment exhibit two diverse peaks for distinct oxygen species. The peak at 532.1 eV demonstrates that a hydroxyl (-OH) group present on the TiO<sub>2</sub> surface, and the other peak at 530.2 eV derives from the saturated oxygen in TiO<sub>2</sub>.<sup>[26]</sup> When the O 1s peaks in XPS spectra are compared, the ratio of the peak deriving from hydroxyl group to the peak originating from saturated oxide (IOH/IO<sub>2</sub>) decreases from a value of 1.74 (pristine TiO<sub>2</sub>) to 0.53 (TiO<sub>2</sub> with HF treatment). This result indicates that the amount of hydroxyl group on the TiO<sub>2</sub> surface can be effectively removed with HF treatment. In the field of fluorine, the XPS spectrum of the TiO<sub>2</sub> with HF treatment shows double peaks, whereas the XPS spectrum of pristine TiO<sub>2</sub> exhibits no obvious signal. The presence of fluorine shows that the fluoride treatment induces chemical fluorination doping on TiO<sub>2</sub>.<sup>[27]</sup> From the XPS results of Ti 2p and F 1s for these two different samples, it can be concluded that the HF treatment resulted in the fluorine incorporation on the TiO<sub>2</sub> surface.

To investigate the effects of fluoride treatment on the TiO<sub>2</sub> layer, density functional theory calculations were used to study the properties of the defects and atomic structures of pristine TiO<sub>2</sub> and TiO<sub>2</sub> with HF treatment. As shown in **Figure S1**, Supporting Information, TiO<sub>2</sub> crystallizes with an anatase structure, and the (101) surface composed of flat Ti-O planes connected by O atoms is its natural cleavage surface. In the actual situation, the undercoordinated Ti on the TiO<sub>2</sub> surface tends to be fully covered with water and interact with water to form up to four hydroxyl groups. To facilitate the calculation, we assumed that the TiO<sub>2</sub> unit adsorbed four hydroxyl groups (OH) on the surface, as shown in **Figure 2a**. The adsorption energy of the fluorine ions was calculated using the equation:  $E_{\text{ads}} = E_{[\text{F-TiO}_2]} - E_{[\text{F}]} - E_{[\text{TiO}_2]}$ .<sup>[28]</sup> **Figure 2a** exhibits the optimized structure of F-TiO<sub>2</sub> after energy relaxation. The adsorption energy of the fluoride ions on the TiO<sub>2</sub> surface was calculated to be -3.64 eV, indicating that fluoride ions easily replace the hydroxyl groups on the surface of the titanium dioxide. To further investigate the effects of HF treatment, we calculated the density of states (DOS) and band structure of diverse (101) TiO<sub>2</sub> surfaces, as shown in **Figure 2b**. According to the theoretical calculations, the bandgap of TiO<sub>2</sub> before and after HF treatment (3.494 eV vs 3.493 eV) did not change significantly. To study the modification of the original electronic structure of TiO<sub>2</sub> caused by HF treatment, we calculated the DOS plots, which are shown in **Figure 2b**. The partial DOS plots indicate that most F 2p states located in the lower-energy range of the

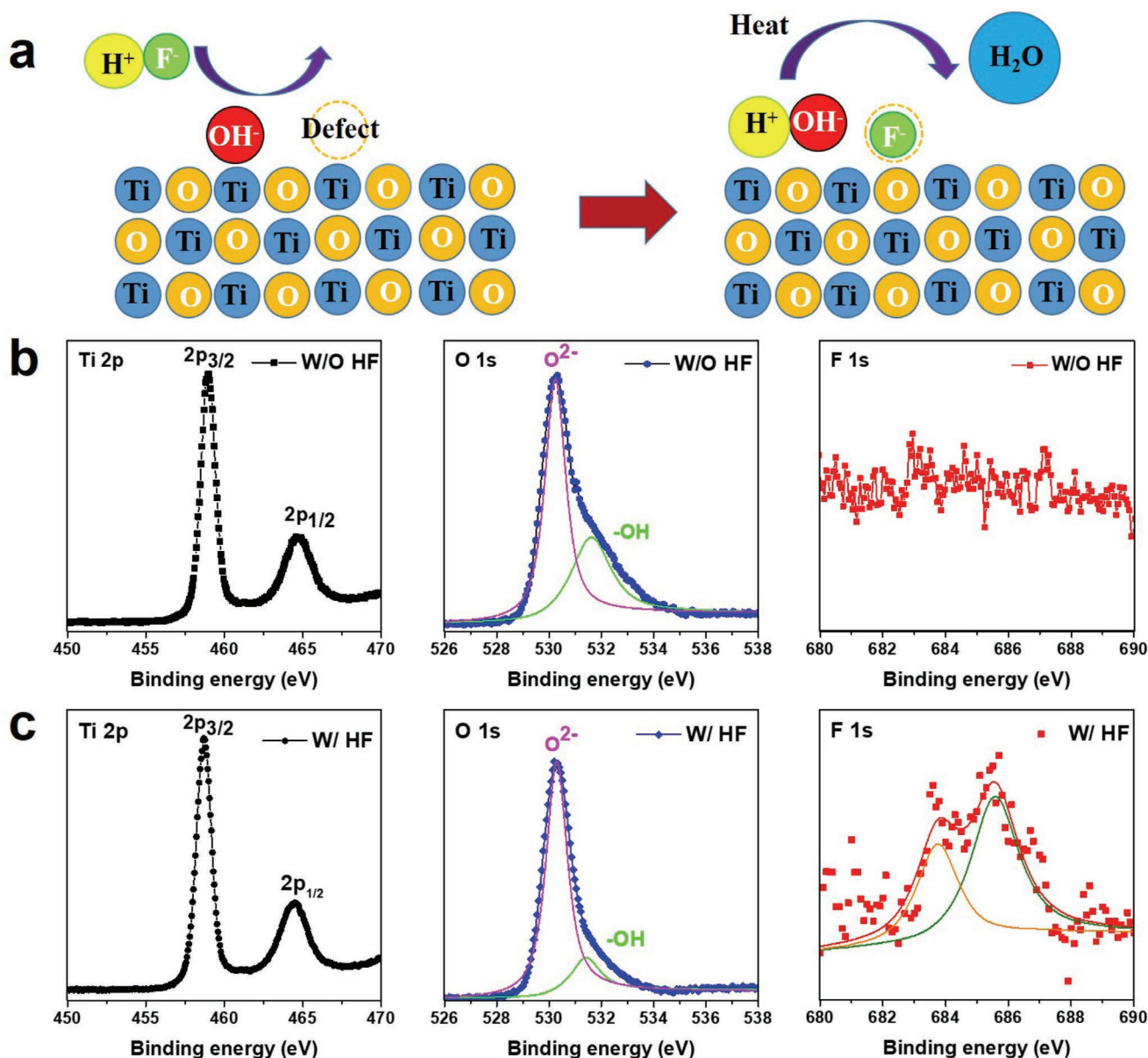


**Figure 1.** a) Schematic diagram of the TiO<sub>2</sub> surface with HF treatment. b, c) XPS spectra of Ti 2p, O 1s, and F 1s for pristine TiO<sub>2</sub> and TiO<sub>2</sub> with HF treatment.

valence band do not make contribution to the formation of bandgap. For electron transport in PSCs, the conduction band minimum (CBM) of TiO<sub>2</sub> plays an important role. Figure 2b reveals that the CBM of TiO<sub>2</sub> with HF treatment is 0.01 eV higher than that of TiO<sub>2</sub> without HF treatment. This result can be attributed to the extra electron highly localized in Ti 3d shell which is induced by fluoride treatment. The increase in the CBM indicates that the energy level difference between TiO<sub>2</sub> and perovskite layer becomes smaller after fluoride treatment and hence can improve charge transport efficiency in PSCs, leading to higher PSC performance.<sup>[29]</sup>

Figure 3a shows the device structure of the PSCs in this work, which consisted of FTO/c-TiO<sub>2</sub>/m-TiO<sub>2</sub> with HF treatment/perovskite/Spiro-OMeTAD/Au, where FTO was used as

the bottom anode, c-TiO<sub>2</sub> and m-TiO<sub>2</sub> with HF treatment were utilized as the ETLs, (FAPbI<sub>3</sub>)<sub>0.95</sub>(MAPbBr<sub>3</sub>)<sub>0.05</sub> was the light absorption layer, 2,2',7,7'-tetrakis [N,N-di(4-methoxyphenyl) amino]-9,9'-spirobifluorene (Spiro-OMeTAD) was constructed as the HTL, and Au was the top cathode. Due to the corrosion and toxicity of HF, it is not suitable to use a conventional spin-coating method for the HF treatment. Therefore, for the fluoride treatment, a simple soaking method was developed to avoid HF solution leakage. The process is described in detail in the Experimental Section. Figure 3b shows a cross-sectional SEM image of the whole PSC device, which exhibits a well-defined multilayer structure with distinct interfaces. We then studied the effect of different ETLs on the perovskite film. Figure S2, Supporting Information, shows the SEM images



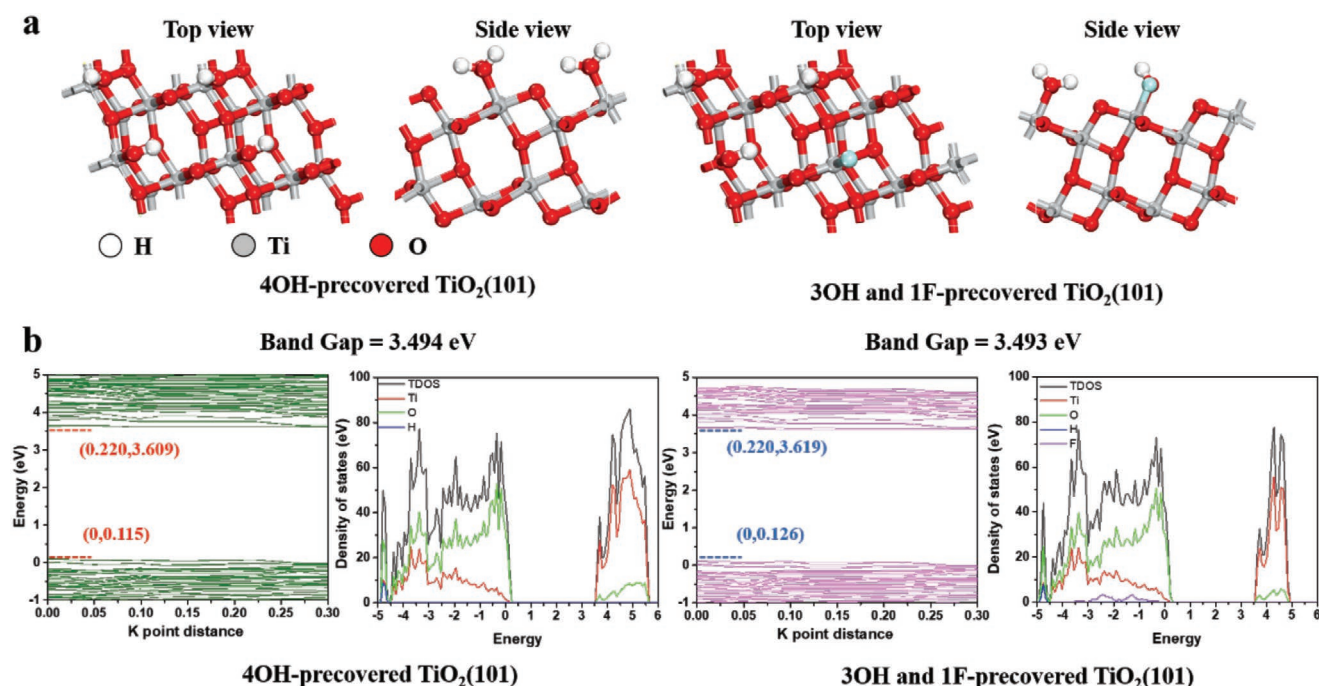


**Figure 2.** a) Top and side views of 4OH-precovered TiO<sub>2</sub>(101) and 3OH- and 1F-precovered TiO<sub>2</sub>(101) structural models. b) Density of states (DOS) and band structure of different (101) TiO<sub>2</sub> surfaces.

of the perovskite film deposited on the surface of TiO<sub>2</sub> film and HF-treated TiO<sub>2</sub> film with the one-step method. Both perovskite films have a compact and smooth morphology with a spot of white phase on the surface, which is PbI<sub>2</sub> formed from the decomposition of perovskite during annealing process.<sup>[30]</sup> A slight PbI<sub>2</sub> on the surface of perovskite film is thought to improve PSC performance by passivating the defect sites

between the perovskite and HTL interface.<sup>[31]</sup> Both perovskite films have a similar thickness and grain size. In addition, the growth of single perovskite crystal grain along the normal direction of the interface could facilitate charge transport in the perovskite layer. As shown in Figure S3, Supporting Information, we used UV photoelectron spectroscopy (UPS) and UV-vis absorption spectra to confirm the energy band structure of the two types of ETL films. The work functions (WFs) of the TiO<sub>2</sub> film and the TiO<sub>2</sub> film with HF treatment are estimated to be 4.31 and 4.19 eV, respectively. These values were obtained by subtracting the excitation energy (21.22 eV) of the He UPS spectra. The valence band spectra indicates that the energy gaps between the Fermi level ( $E_F$ ) and VBM of the TiO<sub>2</sub> film and the HF-TiO<sub>2</sub> film are estimated to be 3.11 and 3.12 eV, respectively. Combining the results of light absorption spectra (Figure S4a, Supporting Information), the CBMs are 4.21 and 4.11 eV and the VBMs are 7.42 and 7.31 eV for the TiO<sub>2</sub> film and the HF-TiO<sub>2</sub> film, respectively. Although the absolute value of CBM improvement is different in theoretical calculation and experiment, the variation trend is consistent, which may reveal the more suitable energy level of TiO<sub>2</sub> after HF treatment. As shown in Figures S4b and S5, Supporting Information, both the bandgap (1.52 eV) and energy level position of perovskite did not exhibit obvious change when the perovskite film was deposited on the TiO<sub>2</sub> W/O and W/HF treatment. In addition, we used UPS to determine the energy level of Spiro-OMeTAD (Figure S6, Supporting Information). The energy band alignment of different functional layers is displayed in Figure 3d. The Fermi energy level of TiO<sub>2</sub> was upshifted by 0.10 eV with the HF treatment, which is attributed to the fluorine doping of TiO<sub>2</sub>. The WF shift after HF treatment could be due to fluorine substitution on the surface of TiO<sub>2</sub>, generating a doping

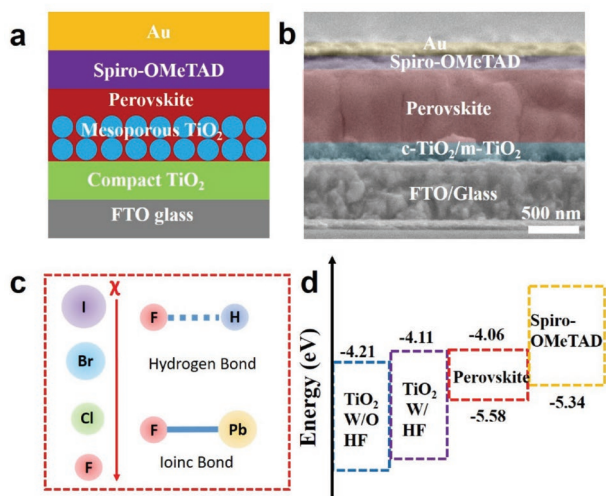


**Figure 3.** a) Schematic diagram of the perovskite solar cells structure. b) Cross-sectional SEM of the perovskite solar cells device. c) Schematic illustration of how the hydrogen bond between the halogen and FA ions is enhanced and how the ionic bond between the halogen and metal ions is strengthened by increasing halogen electronegativity. d) Illustration of the energy band alignment of TiO<sub>2</sub>, TiO<sub>2</sub> with HF treatment, and the perovskite layer.

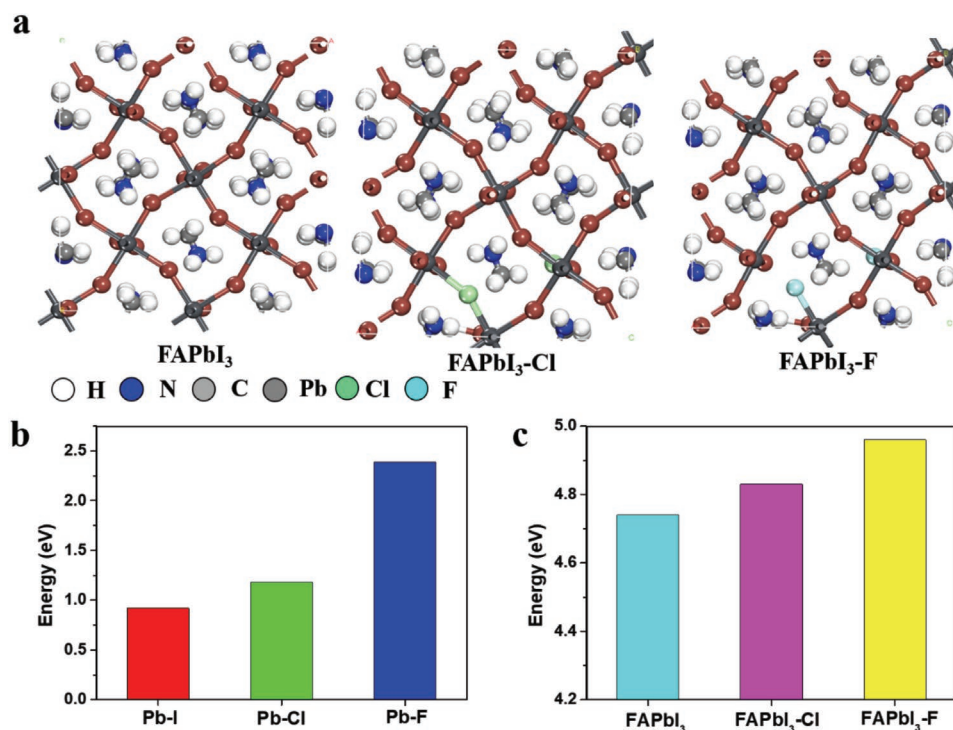


**Figure 4.** a) Side views of the FAPbI<sub>3</sub>, FAPbI<sub>3</sub>-Cl, and FAPbI<sub>3</sub>-F models. b) Formation energy of Pb-I, Pb-Cl, and Pb-F antisite defects in clean FAPbI<sub>3</sub>, FAPbI<sub>3</sub>-Cl, and FAPbI<sub>3</sub>-F. c) Formation energy of FA vacancy in FAPbI<sub>3</sub>, FAPbI<sub>3</sub>-Cl, and FAPbI<sub>3</sub>-F.

energy level near the CBM of TiO<sub>2</sub>. Compared to the TiO<sub>2</sub> film, the energy band of the TiO<sub>2</sub> with HF treatment film is more beneficial to facilitate the charge extraction from the perovskite, which is consistent with the results of theoretical calculation. On the other hand, the energy level difference between the perovskite and Spiro-OMeTAD layers is 0.24 eV, which is suitable for the charge transportation and causes a minor energy loss.

As used in our design, F<sup>-</sup> can not only passivate the defects on the surface of TiO<sub>2</sub> but also immobilize the cations and anions in the perovskite. In the halide series I, Br, Cl, and F (Figure 3c), the electronegativity increases while the ionic radius decreases.<sup>[32]</sup> This leads to increased chemical bonding between the halide anions and the FA and Pb cations. As reported by previous literature, the electronic properties of perovskite films can be changed with Cl<sup>-</sup> ions doping or defect passivation at grain boundaries.<sup>[33,34]</sup> Because fluoride ions have the highest electronegativity, high defect passivation effect can be originated from strong hydrogen bonding (N-H...F) with FA<sup>+</sup> cations and ionic bonding with Pb<sup>2+</sup>, which also leads to the immobilization of halide anions and organic cations.<sup>[35]</sup> To gather more atomistic information as for the effects of F<sup>-</sup> treatment on the efficiency and stability of PSCs, the relative F<sup>-</sup> incorporation energy on the surface of the perovskite was calculated by using DFT. To investigate the influence of different halogen ions, we used chloride ions as a comparison (Figure 4a). As shown in Figure 4b, incorporating F ions into the perovskite lattice is extremely difficult, as the ions have a trend to stay on the surface. Additionally, incorporating F ions on the surface can change the local bonding energy at the surface of the perovskite layer. Based on theoretical calculations,

the F ions increase the formation energy for different kinds of defect. For instance, the formation energies of Pb-I, Pb-Cl, and Pb-F antisite defects are 0.92, 1.18, and 2.39 eV, respectively. Therefore, Pb-F antisite defects at deep-level are less than Pb-I and Pb-Cl antisite defects, which could contribute to higher charge transporting efficiency. This result can be attributed to two main factors. The first one is that the F ion forms stronger ionic bonds with Pb compared to Cl and I ions, which may restrict the movement of lead and fluoride ions. The second one is that fluoride ion has a smaller radius than chloride and iodide ions, impeding the entrance of Pb ion. In addition, other research has shown that strong hydrogen bonds can be formed between FA ions closest to an F site and the F ion. To better understand the effects of F ion incorporation, we used theoretical calculation to obtain the formation energies of FA cation vacancies on the clean perovskite surface and the surfaces incorporated with Cl<sup>-</sup> or F<sup>-</sup> ions (Figure 4c). When compared to the pristine perovskite (4.74 eV), the FA vacancy formation energy in FAPbI<sub>3</sub>-Cl (4.83 eV) increased by only 0.09 eV, whereas the FA vacancy formation energy in FAPbI<sub>3</sub>-F (4.96 eV) increased by 0.22 eV. Therefore, the introduction of F markedly reduced the formation of FA vacancies on the surface. To verify whether the F<sup>-</sup> ions interact with the amine group (FA) in the perovskite film, we measured <sup>1</sup>H proton nuclear magnetic resonance (<sup>1</sup>H NMR) spectra. As shown in Figure S7, Supporting Information, we can see that a significant chemical shift has occurred in the sample with HF passivation from the <sup>1</sup>H NMR spectrum. This is due to the interaction between F and organic groups (FA) to form a hydrogen bond (NH...F), which effectively reduces the diffusion of organic cations and improves the stability of the devices. In summary, the addition of F to the surface of

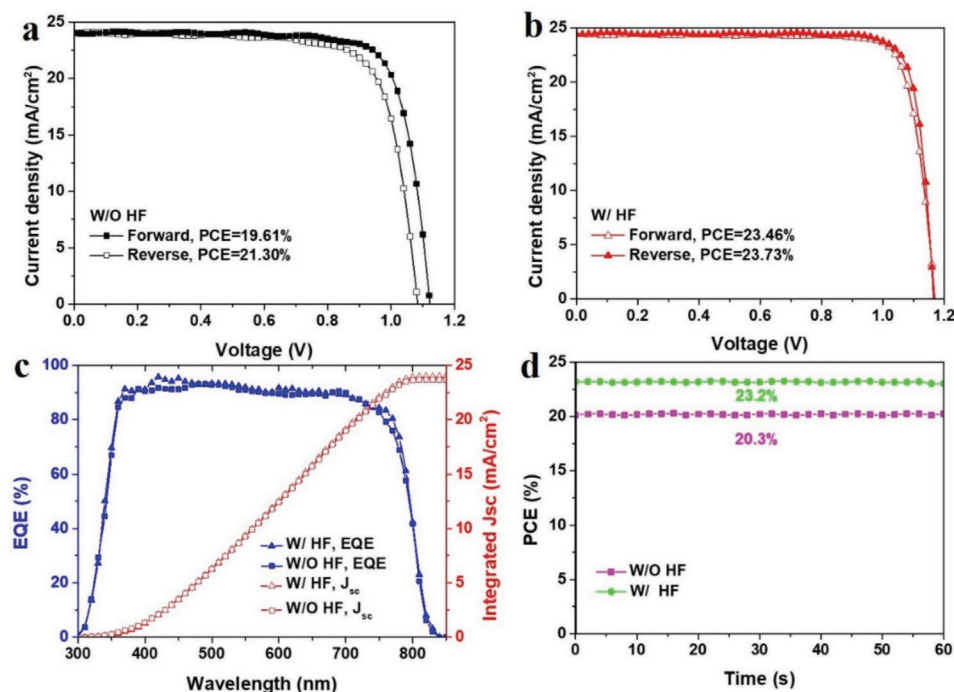


**Figure 5.** a,b)  $J$ - $V$  curves of the champion PSC device without and with HF treatment under reverse and forward scanning direction. c) The corresponding EQE spectra and the integrated  $J_{sc}$ . d) Stabilized PCE of the corresponding devices measured at a fixed voltage.

perovskite stabilized the local structure through enhanced hydrogen bonds with FA ions and bonding with Pb.

To study the effect of HF treatment on PSC device performance, the current density–voltage curves of PSCs without and with HF passivation were measured. The detailed photovoltaic parameters are shown in Table S1, Supporting Information. As shown in **Figure 5a,b**, the best device without HF passivation has a PCE of 21.30% with an open-circuit voltage ( $V_{oc}$ ) of 1.12 V, a short-circuit current density ( $J_{sc}$ ) of 24.05 mA cm<sup>-2</sup>, and a fill factor (FF) of 78.7% under the reverse scan, and a PCE of 19.61% with a  $V_{oc}$  of 1.08 V, a  $J_{sc}$  of 24.01 mA cm<sup>-2</sup>, and an FF of 75.8% under the forward scan. The hysteresis index (defined by  $PCE_{reverse} - PCE_{forward} / PCE_{reverse}$ ) is 0.079. In contrast, for PSCs with HF passivation, the best device has a  $V_{oc}$  of 1.17 V, a  $J_{sc}$  of 24.31 mA cm<sup>-2</sup>, and an FF of 83.5% under the reverse scan, yielding a PCE of 23.73%. The PSC device yields a PCE of 23.46% under the forward scan. With HF passivation, the hysteresis index of 0.012 is negligible. **Figure S8**, Supporting Information, shows the statistical distribution of the PCE and FF for the PSCs based on the TiO<sub>2</sub> film and the HF-TiO<sub>2</sub> film, demonstrating a significant improvement in the PCE and FF. As shown in **Figure 5c**, the integrated  $J_{sc}$  calculated from the external quantum efficiency (EQE) spectra for the PSCs without and with HF passivation are 23.8 and 24.1 mA cm<sup>-2</sup>, respectively, which is consistent with the  $J_{sc}$  values measured from the  $J$ - $V$  curves. **Figure 5d** shows the stabilized PCEs without and with HF passivation at a fixed voltage. This result also demonstrates that the PCE can be significantly improved by the passivating effects of HF treatment. The short-circuit current density ( $J_{sc}$ ) increases only slightly in HF-treated devices, whereas the open-circuit voltage ( $V_{oc}$ ) and fill factor (FF) improve

dramatically. The improvement in the  $V_{oc}$  is mainly due to two crucial factors. One factor is the effective interfacial defect passivation derived from fluoride. With the introduction of fluoride and reduced trap density, nonradiative recombination during the working process is greatly restricted. The other factor is that HF treatment resulted in a more suitable energy level alignment of TiO<sub>2</sub>. A smaller energy gap between TiO<sub>2</sub> and the perovskite layers could greatly minimize internal energy loss during electron extraction while ensuring efficient electron extraction. The remarkably increased FF is due to more efficient contact, enhanced charge carrier lifetime, and decreased nonradiative recombination centers in perovskite films. From the  $I$ - $V$  characteristics of the FTO/TiO<sub>2</sub>/Au devices shown in **Figure S10**, Supporting Information, the better electron mobility of TiO<sub>2</sub> W/HF treatment can induce faster electron transport, also leading to the improved FF. The enhancement of the  $J_{sc}$  is mainly due to improved electron extraction and transport efficiency, as discussed above. Additionally, an increased TiO<sub>2</sub> electron mobility and a higher matching energy level position improve the  $J_{sc}$  value of PSC devices. Furthermore, the efficiencies of PSCs with different HF concentrations were systematically studied. As shown in **Figure S9**, Supporting Information, the efficiencies of all PSC devices were improved as the HF concentration increased from 10 to 50 mM for the HF-treated m-TiO<sub>2</sub> film. When the concentration was increased to 100 mM, the performance of the PSCs became insensitive to the HF concentration. The first increase in HF concentration eliminates OH<sup>-</sup> from the TiO<sub>2</sub> film by reacting with the -OH group on the TiO<sub>2</sub> surface to form water (H<sub>2</sub>O). It appears that a small concentration of F<sup>-</sup> ions effectively facilitate the removal of -OH on the TiO<sub>2</sub> surface and lead to passivation for deep-level defects on the



bottom surface of the perovskite layer, whereas an overly high concentration of  $F^-$  may hinder charge transport. As a result, a molar concentration of 50 mM HF led to the best PCE. It is important to emphasize that the effect of  $F^-$  differs from that of other halide ions. To demonstrate this, we fabricated PSCs treated with other haloid acids. The corresponding PCEs with HF treatment were clearly better than the untreated devices, HCl-treated devices, and HBr-treated devices (Figure S11a, Supporting Information). Additionally, these devices have clear  $J-V$  hysteresis (larger hysteresis index), whereas the HF-treated devices have an almost negligible  $J-V$  hysteresis (Figure S11b, Supporting Information). Mobile ions and their accumulation through defects at the interface between the  $TiO_2$  and perovskite are reported to be responsible for  $J-V$  hysteresis. The surface defects tend to move and redistribute under the effect of the electric field in PSCs device, resulting in defect migration and further leading to the device hysteresis. As a result, passivating the surface defects is an effective strategy to reduce device hysteresis. When using HF, due to the large number of defects passivating the F-defects, ions in perovskite are bonded and are therefore mostly localized. The above analysis emphasizes that, compared to other halides, fluoride has a unique ability to passivate both defects on the  $TiO_2$  surface and the bottom surface of the perovskite layer. To prove the generality of the results, we also utilize  $NH_4F$  as an additive to fabricate PSCs. We fabricated  $NH_4F$ -treated PSCs through the same process used for fabricating HF-treated PSCs. Figure S12, Supporting Information, shows that  $NH_4F$ -treated PSCs exhibit a slightly lower PCE than HF-treated PSCs. Moreover, both  $NH_4F$ - and

HF-treated PSCs exhibit negligible hysteresis, revealing that  $NH_4F$  is also available to passivate the defects at the interface, leading to efficient and stable PSC devices. The above analysis shows that fluoride ions are applicable for the passivation of both defects on the  $TiO_2$  surface and the bottom surface of the perovskite layer, and that they can be combined with a variety of cations. We note that the  $H^+$  also plays a significant role in the passivation process because it can effectively remove the hydroxyl groups on the surface of  $TiO_2$ , leading to the better passivation effect and enhanced light stability.

We studied charge-transfer properties to find out the role of HF treatment at the perovskite/ $TiO_2$  interface by performing a series of photoluminescence (PL) spectroscopy measurements. As shown in Figure 6a, the steady-state PL spectra indicate that HF-treated samples had a higher quenching efficiency of 85% (versus the pristine perovskite film), while  $TiO_2$  without HF treatment had a quenching efficiency of 73%, showing that the modified  $TiO_2$  surface with HF treatment is more beneficial to the electron extraction from the perovskite film. The corresponding time-resolved PL (TRPL) decay curves were shown in Figure 6b. These curves were fitted with a biexponential decay function, generating a fast decay ( $\tau_1$ ) and a slow decay ( $\tau_2$ ) component, as described in Table S2, Supporting Information. The photophysical interpretation for perovskite/charge transporting layer interfaces is commonly considered that  $\tau_1$  derives from charge carrier quenching by charge selective layers, whereas  $\tau_2$  originates from radiative recombination in the bulk perovskite.<sup>[36]</sup> The lifetimes of sample with HF treatment were calculated as a  $\tau_1$  value of 21 ns and a  $\tau_2$  value of 143 ns, whereas the

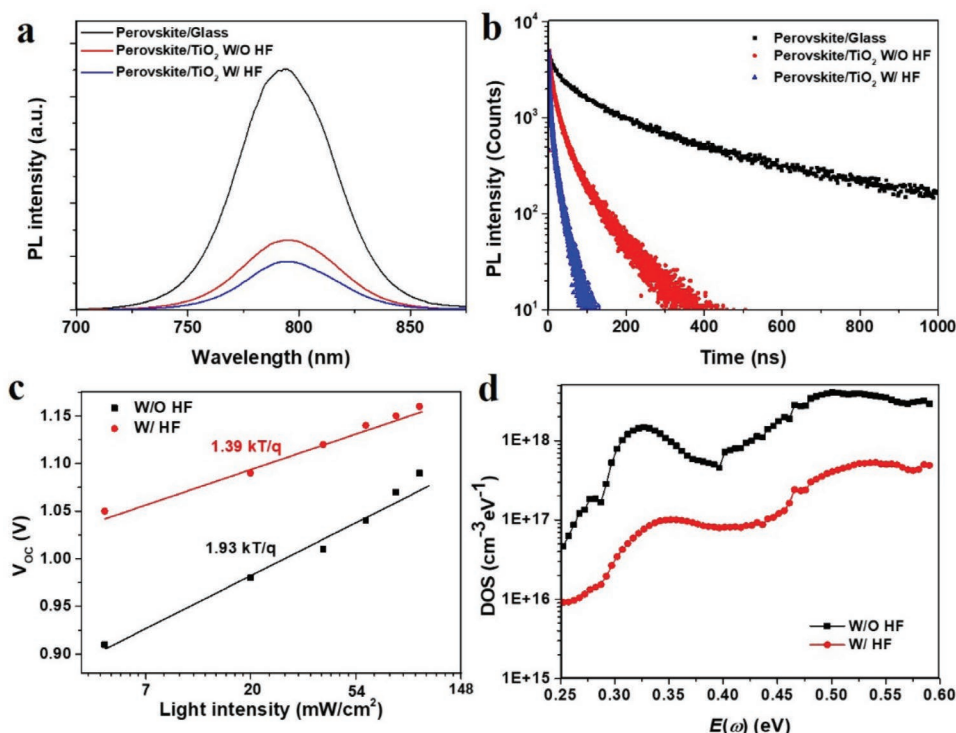


**Figure 6.** a) Steady-state photoluminescence spectra and b) time-resolved photoluminescence decay curves of perovskite films on glass,  $TiO_2$  without and with HF treatment substrates. c)  $V_{oc}$  versus light intensity for the PSCs using  $TiO_2$  without and with HF treatment. d) Trap density of states (tDOS) calculated from the TAS measurement of PSCs without and with HF treatment.

control sample exhibited a larger  $\tau_1$  of 32 ns and a  $\tau_2$  of 246 ns, demonstrating that the HF treatment results in faster electron extraction. The shorter carrier lifetime and improved extraction can be attributed to two main factors, the first one is the improved perovskite quality with the effect of defect passivation and the second one is the better energy alignment between the  $\text{TiO}_2$  and perovskite in consistent with the results from Figure 3d. We can see the light intensity-dependent  $V_{oc}$  for the two ETL-based devices in Figure 6c. The slope of the  $V_{oc}$  versus light intensity curve reduces from  $1.93 \text{ kT q}^{-1}$  for the  $\text{TiO}_2$  film-based device to  $1.39 \text{ kT q}^{-1}$  for the HF-treated  $\text{TiO}_2$  film-based device. The deviation between the value of the slope and  $\text{kT q}^{-1}$  is related to the degree of trap-assisted nonradiative recombination. The lessened slope indicates that the trap-state density is effectually suppressed. Thermal admittance spectroscopy (TAS) was used to further investigate the effect of defect passivation. Figure 6d shows the values of the trap density of states (tDOS) calculated from the TAS analysis for the PSCs based on  $\text{TiO}_2$  without and with HF treatment. Previous studies have demonstrated that the region with an energy greater than 0.30 eV is denoted as the trap states on the surface and grain boundaries of the perovskite layer and the region with an energy less than 0.30 eV is denoted as the shallow trap state responding to the defect concentration in the perovskite bulk.<sup>[37]</sup> The concentration of shallow trap states is higher in the PSC without HF treatment than in the PSC with HF treatment. This demonstrated that the perovskite film without HF treatment have more defects in the bulk. Compared to the PSCs without HF treatment, the tDOS of the PSCs with HF treatment was reduced by almost two orders of magnitude. This result demonstrated that HF treatment has an effective passivation effect on

deep trap states in perovskite films. The decreased trap states could be attributed to the lower concentration of deep-level defects at the interface between  $\text{TiO}_2$  and perovskite layer after HF treatment.

Long-term stability of PSCs under various working conditions, such as humidity, light irradiation, and heat, are crucial for their commercialization. In this work, we scientifically studied the effect of HF treatment on device stability under three conditions: humidity, light irradiation, and heat. Previous research has shown that defects in perovskite films have a high diffusivity and are more impressionable due to moisture and oxygen. Here, HF was thus expected to neutralize the charges due to its strong interaction with the ionic defects, thereby inhibiting moisture and oxygen permeating through these defects. To testify the deduction, we measured the humidity stability of PSCs with and without HF treatment. We investigated the effects of  $\text{F}^-$  passivation on PSC devices during aging in both low (<30%) and high humidity environments (>70%). First, we recorded the efficiency of the unencapsulated PSCs with and without HF treatment in a dark environment at low humidity (RH < 30%). Figure 7a shows that the performance of the PSCs without HF treatment clearly showed faster decay after storage in low-humidity air for 1400 h. Considering practical applications, PSCs should remain stable in high humidity environments. Therefore, to study the effects of HF treatment at high humidity, we measured the efficiency of PSCs that were encapsulated by UV curable resin at a relative humidity >70% (Figure 7b). The PSCs with HF treatment retained nearly 91% of the initial PCE storing at a high humidity environment for over 1400 h, showing higher humidity stability than that of PSCs without HF treatment under the same conditions.

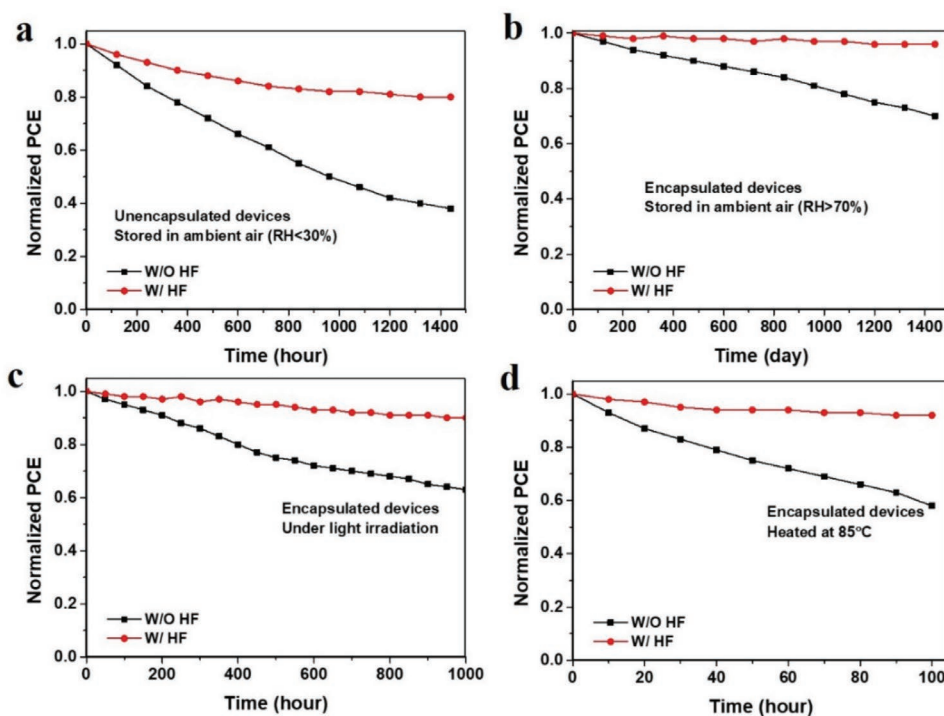


**Figure 7.** a) Humidity stability of unencapsulated devices under RH <30%. b) Humidity stability of encapsulated devices under RH >70%. c) Light illumination stability of encapsulated devices. d) Thermal stability of encapsulated devices at 85 °C.



Defects at the interface usually provided a pathway for moisture and oxygen in air, resulting in fast degradation of PSCs. These results demonstrate that the PSCs with F<sup>-</sup> passivation have excellent environmental stability, which can be attributed to improved crystal quality and reduced defects at the interface and in the perovskite film after F<sup>-</sup> passivation. In addition, to study the light stability of PSCs, we recorded their PCEs under continuous light illumination at 100 mW cm<sup>-2</sup>. As reported in previous literature, a rapid degradation in the performance caused by the exposure to UV light is the main issue of TiO<sub>2</sub>-based device.<sup>[38]</sup> Due to the wider bandgap, SnO<sub>2</sub> absorbs less UV light and is thus more robust than TiO<sub>2</sub> under sunlight. However, mesoporous TiO<sub>2</sub> can offer more contact area and stable template for the growth of perovskite film, which may lead to better reproducibility and higher efficiency. To address the light degradation issue, we developed HF to reduce the amount of hydroxy and undercoordinated Ti on the surface of TiO<sub>2</sub>, which can highly reduce the degradation caused by UV light. As shown in Figure 7c, without HF treatment, the PSCs exhibit complete decay of PSCs after 1000 h of light irradiation, due to the photo-oxidation of perovskite under light irradiation. However, HF treatment can effectively passivate the defects on the surface of TiO<sub>2</sub>, resulting in less photogenerated charges. As expected, PSCs with HF treatment maintained 92% of their initial efficiency for 1000 h under light irradiation, which is higher than that of SnO<sub>2</sub> and other TiO<sub>2</sub>-based devices (Table S3, Supporting Information). This result demonstrates that HF treatment can effectively passivate defects in both the TiO<sub>2</sub> and the perovskite film, resulting in increased light stability. Furthermore, the thermal stability of PSC was tested at 85 °C. At high temperatures, alkyl amine gases and volatile hydrogen halide are easier to escape from perovskite films, causing rapid thermal degradation of PSCs.<sup>[39]</sup> As shown in Figure 7d, PSCs with HF treatment outperformed the reference cells without HF treatment in terms of stability. PSCs with HF treatment can retain 90% of their initial PCE after 100 h. Nevertheless, the PCEs of devices without HF treatment dropped below 70% of their initial values in less than 100 h. These results further demonstrate that the passivation effect of HF treatment for defects in both the TiO<sub>2</sub> and perovskite layer resulted in considerable improvements in the thermal stability of PSC devices.

### 3. Conclusion

In conclusion, we have demonstrated a bifunctional strategy through fluoride treatment for simultaneously passivating defects in both the TiO<sub>2</sub> and the perovskite layer. First, fluoride treatment can be used to improve the Fermi energy level of TiO<sub>2</sub> and lead to more efficient electrons transferring from the perovskite film to TiO<sub>2</sub> layer. At the same time, the interfacial passivation caused by fluoride treatment led to decreased energy losses in PSC device, contributing to enhanced efficiency. Due to a better energy band alignment and interface passivation, PSC device with fluoride-treated TiO<sub>2</sub> film as the ETL can achieve a PCE of over 23.7% with negligible hysteresis. Furthermore, the stability of PSCs can be obviously enhanced. These results demonstrate the key effect of the defects' passivation

both on the surface of ETL and interface and afford a new idea for the development of high efficiency and stability PSCs.

### 4. Experimental Section

**Synthesis:** Formamidine iodide (FAI) was synthesized by reacting 10 g of formamidine acetate (99%, Alfa Aesar) and 15 mL of hydroiodic acid (57% in water, Aldrich) in a 150 mL round-bottom flask at 60 °C temperature and 1 mbar pressure for 1 h with rotation. Methylammonium bromide (MABr) was synthesized by reacting 28 mL of methylamine solution (40 wt% in H<sub>2</sub>O) and 52 mL of hydrobromic acid (ACS reagent 48%) in a 150 mL round flask in an ice-water bath for 3 h with stirring. It was then rotated at 60 °C temperature and 1 mbar pressure for 3 h. The products were first dissolved in ethanol, and then recrystallized from diethyl ether. Finally, they were dried at RT in a vacuum oven for 48 h. Methylamine hydrochloride (MAH) was purified by recrystallization method and dried at room temperature in a vacuum oven for 48 h. Formamidine lead iodide (FAPbI<sub>3</sub>) was synthesized by reacting FAI, lead (II) iodide, and 8 mL of 2-methoxyethanol in a 40 mL beaker with stirring. The mixed solution was heated up to 120 °C and then precipitated by retrograde method. FAPbI<sub>3</sub> black powder was filtered and then dried at 150 °C for 20 min. Methylammonium lead bromide (MAPbBr<sub>3</sub>) was synthesized by reacting 1:1 molar ratio of synthesized MABr and PbBr<sub>2</sub> (Aldrich) in 6 mL of dimethylformamide (DMF). Single crystalized MAPbBr<sub>3</sub> in a sealed solution was filtered and baked at 100 °C for 30 min.

**Solar Cell Fabrication:** Etched F-doped SnO<sub>2</sub> (FTO) was sonicated in detergent, DI water, acetone, and isopropanol, respectively. A thin compact TiO<sub>2</sub> layer was deposited onto a FTO substrate by spraying titanium diisopropoxide bis(acetylacetonate) in ethanol (1:20 volume ratio) at 450 °C. A 150 nm layer of mesoporous (m)-TiO<sub>2</sub> was spin-coated at 3000 rpm onto the substrate using commercial TiO<sub>2</sub> paste diluted with 2-methoxyethanol, and then annealed at 500 °C for 1 h in air. For the fluorine treatment, the TiO<sub>2</sub> substrates were first covered with Scotch tape to protect the part of FTO/glass and then soaked in HF acid solution with different concentrations for 5 min. After that, the fluorine treated samples were rinsed in a solution of ethanol and DI water (1:1 in volume) for 5 min and then blow-dried with a nitrogen flow. FAPbI<sub>3</sub> (1.26 M) containing 5 mol% MAPbBr<sub>3</sub> and 46 mol% MAH was dissolved in a mixture of DMSO and DMF (1:8 volume ratio) at 60 °C. The perovskite film was fabricated by spin-coating the resulting solution onto the m-TiO<sub>2</sub> layer at 1000 and 5000 rpm for 5 and 20 s, respectively. During the second spin-coat step, 1 mL diethyl ether was dropped on the substrate as anti-solvent. Subsequently, the substrate was put on a hot plate to be heated at 150 °C for 15 min and then at 100 °C for 10 min to produce (FAPbI<sub>3</sub>)<sub>0.95</sub>(MAPbBr<sub>3</sub>)<sub>0.05</sub> mixed halide perovskite thin film. The hole transport layer was spin-coated on the surface of perovskite film at 3000 rpm for 30 s by using the Spiro-OMeTAD solution. The Spiro-OMeTAD solution was prepared by dissolving 72.3 mg Spiro-OMeTAD, 35 µL bis (trifluoromethane) sulfonamide lithium salt (Li-TFSI, 260 mg mL<sup>-1</sup> in acetonitrile), and 29 µL 4-*tert*-butylpyridine in 1 mL chlorobenzene. Finally, a gold film with 80-nm thickness was constructed on the top of Spiro-OMeTAD using thermal evaporation.

**Characterization:** The J-V characteristics of the PSC devices were measured by using a Keithley 2400 source meter under light illumination. The intensity of light was set at 100 mW cm<sup>-2</sup> (AM 1.5G) by a solar simulator (Newport, Oriel Sol3A Class AAA). A calibrated silicon cell certified by NREL was used as reference cell. The step voltage was 0.02 V and the delay time was set as 40 ms. An aperture of 0.09 cm<sup>2</sup> was used to calibrate the active area. The film morphologies were measured using a scanning electron microscope (ZEISS Merlin). The optical properties of the films were measured by using UV-vis spectroscopy (PerkinElmer LAMBDA 950). Steady-state PL and TRPL spectra were measured using commercial time-correlated single photon counting setup (Edinburgh FLS 1000). Electrochemical impedance spectroscopy was conducted using electrochemical workstation (CH660). The solar

cells were encapsulated with a cover glass and UV epoxy (Three Bond) and then were cured under an UV light-emitting diode lamp for 5 min (Figure S13, Supporting Information). All the stability measurements were processed in ambient air, where the ambient temperature was around 25 °C. For the humidity stability test, the samples were stored in a home-made box with a humidity sensor, a controller, a humidifier, and a dehumidifier to keep the ambient humidity around the set value. For the thermal stability test, the samples were put on a hot-plate to achieve setting temperature. For the light stability, as shown in Figure S14, Supporting Information, cooling system was used to keep the surface temperature of samples at around 25 °C. All the stability tests were measured by using three samples with same types and the results were averaged to reduce deviation.

## Supporting Information

Supporting Information is available from the Wiley Online Library or from the author.

## Acknowledgements

This work was supported by the National Key Research and Development Project funding from the Ministry of Science and Technology of China (Grant Nos. 2021YFB3800100 and 2021YFB3800101), the National Natural Science Foundation of China (Grant Nos. 61904076, 62174078, and U19A2089), the Natural Science Foundation of Guangdong Province (Grant Nos. 2020A1515010980 and 2019B1515120083), the Peacock Team Project funding from the Shenzhen Science and Technology Innovation Committee (Grant No. KQTD2015033110182370), the Key Fundamental Research Project funding from the Shenzhen Science and Technology Innovation Committee (Grant No. JCYJ20200109141014474), the Shenzhen Engineering R&D Center for Flexible Solar Cells Project funding from Shenzhen Development and Reform Committee (Grant No. 2019-126), and the Guangdong-Hong Kong-Macao Joint Laboratory (Grant No. 2019B121205001).

## Conflict of Interest

The authors declare no conflict of interest.

## Data Availability Statement

The data that support the findings of this study are available from the corresponding author upon reasonable request.

## Keywords

defects' passivation, fluoride treatments, perovskite solar cells

Received: March 19, 2022

Revised: June 3, 2022

Published online:

- [4] S.-H. Turren-Cruz, A. Hagfeldt, M. Saliba, *Science* **2018**, 362, 449.
- [5] J. Jeong, M. Kim, J. Seo, H. Lu, P. Ahlawat, A. Mishra, Y. Yang, M. A. Hope, F. T. Eickemeyer, M. Kim, Y. J. Yoon, I. W. Choi, B. P. Darwich, S. J. Choi, Y. Jo, J. H. Lee, B. Walker, S. M. Zakeeruddin, L. Emsley, U. Rothlisberger, A. Hagfeldt, D. S. Kim, M. Gratzel, J. Y. Kim, *Nature* **2021**, 592, 381.
- [6] H. Chen, F. Ye, W. Tang, J. He, M. Yin, Y. Wang, F. Xie, E. Bi, X. Yang, M. Gratzel, L. Han, *Nature* **2017**, 550, 92.
- [7] B.-w. Park, H. W. Kwon, Y. Lee, D. Y. Lee, M. G. Kim, G. Kim, K.-j. Kim, Y. K. Kim, J. Im, T. J. Shin, S. I. Seok, *Nat. Energy* **2021**, 6, 848.
- [8] M. Bauer, H. Zhu, T. Baumeler, Y. Liu, F. T. Eickemeyer, C. Lorenz, E. Mena-Osteritz, D. Hertel, S. Olthof, S. M. Zakeeruddin, K. Meerholz, M. Graetzel, P. Baeuerle, *Adv. Energy Mater.* **2021**, 11, 2003953.
- [9] X. Shi, Y. Ding, S. Zhou, B. Zhang, M. Cai, J. Yao, L. Hu, J. Wu, S. Dai, M. K. Nazeeruddin, *Adv. Sci.* **2019**, 6, 1901213.
- [10] X. Lin, J. Lu, S. R. Raga, D. P. McMeekin, Q. Ou, A. D. Scully, B. Tan, A. S. R. Chesman, S. Deng, B. Zhao, Y.-B. Cheng, U. Bach, *Adv. Energy Mater.* **2021**, 11, 2100053.
- [11] H. Tan, A. Jain, O. Voznyy, X. Lan, F. P. G. de Arquer, J. Z. Fan, R. Quintero-Bermudez, M. Yuan, B. Zhang, Y. Zhao, F. Fan, P. Li, L. N. Quan, Y. Zhao, Z.-H. Lu, Z. Yang, S. Hoogland, E. H. Sargent, *Science* **2017**, 355, 722.
- [12] T. Webb, S. J. Sweeney, W. Zhang, *Adv. Funct. Mater.* **2021**, 31, 2103121.
- [13] Z. Dai, S. K. Yadavalli, M. Chen, A. Abbaspourtamijani, Y. Qi, N. P. Padture, *Science* **2021**, 372, 618.
- [14] T. Leijtens, G. E. Eperon, S. Pathak, A. Abate, M. M. Lee, H. J. Snaith, *Nat. Commun.* **2013**, 4, 2885.
- [15] B. Chen, H. Chen, Y. Hou, J. Xu, S. Teale, K. Bertens, H. Chen, A. Proppe, Q. Zhou, D. Yu, K. Xu, M. Vafaie, Y. Liu, Y. Dong, E. H. Jung, C. Zheng, T. Zhu, Z. Ning, E. H. Sargent, *Adv. Mater.* **2021**, 33, 2103394.
- [16] L. Gao, H. Su, Z. Xu, Y. Hu, J. Zhang, S. Liu, *Sol. RRL* **2021**, 5, 2100416.
- [17] S. Leng, L. Wang, X. Wang, Z. Zhang, J. Liang, Y. Zheng, J. Jiang, Z. Zhang, X. Liu, Y. Qiu, C.-C. Chen, *Sol. RRL* **2021**, 5, 2100285.
- [18] Q. Yang, X. Wang, S. Yu, X. Liu, P. Gao, X. Hu, G. Hou, S. Chen, X. Guo, C. Li, *Adv. Energy Mater.* **2021**, 11, 2100493.
- [19] Z. Xiong, X. Chen, B. Zhang, G. O. Odunmbaku, Z. Ou, B. Guo, K. Yang, Z. Kan, S. Lu, S. Chen, N. A. N. Ouedraogo, Y. Cho, C. Yang, J. Chen, K. Sun, *Adv. Mater.* **2022**, 34, 2106118.
- [20] Z. Xiong, L. Lan, Y. Wang, C. Lu, S. Qin, S. Chen, L. Zhou, C. Zhu, S. Li, L. Meng, K. Sun, Y. Li, *ACS Energy Lett.* **2021**, 6, 3824.
- [21] F. Gao, C. Luo, X. Wang, Q. Zhao, *Small Methods* **2021**, 5, 2100856.
- [22] X. Zheng, B. Chen, J. Dai, Y. Fang, Y. Bai, Y. Lin, H. Wei, X. C. Zeng, J. Huang, *Nat. Energy* **2017**, 2, 17102.
- [23] H. Wang, F. Li, P. Wang, R. Sun, W. Ma, M. Chen, W. Miao, D. Liu, T. Wang, *Adv. Energy Mater.* **2020**, 10, 2000615.
- [24] M. Kim, I.-W. Choi, S. J. Choi, J. W. Song, S.-I. Mo, J.-H. An, Y. Jo, S. Ahn, S. K. Ahn, G.-H. Kim, D. S. Kim, *Joule* **2021**, 5, 659.
- [25] H. Lu, W. Tian, B. Gu, Y. Zhu, L. Li, *Small* **2017**, 13, 1701535.
- [26] X. Yao, J. Liang, Y. Li, J. Luo, B. Shi, C. Wei, D. Zhang, B. Li, Y. Ding, Y. Zhao, X. Zhang, *Adv. Sci.* **2017**, 4, 1700008.
- [27] E. H. Jung, B. Chen, K. Bertens, M. Vafaie, S. Teale, A. Proppe, Y. Hou, T. Zhu, C. Zheng, E. H. Sargent, *ACS Energy Lett.* **2020**, 5, 2796.
- [28] P. Zhou, X. Zhu, J. Yu, W. Xiao, *ACS Appl. Mater. Interfaces* **2013**, 5, 8165.
- [29] C. Ma, B. Kim, S.-W. Kim, N.-G. Park, *Energy Environ. Sci.* **2021**, 14, 374.
- [30] H. Wang, Z. Wang, Z. Yang, Y. Xu, Y. Ding, L. Tan, C. Yi, Z. Zhang, K. Meng, G. Chen, Y. Zhao, Y. Luo, X. Zhang, A. Hagfeldt, J. Luo, *Adv. Mater.* **2020**, 32, 2000865.

[1] A. Kojima, K. Teshima, Y. Shirai, T. Miyasaka, *J. Am. Chem. Soc.* **2009**, 131, 6050.

[2] M. M. Lee, J. Teuscher, T. Miyasaka, T. N. Murakami, H. J. Snaith, *Science* **2012**, 338, 643.

[3] J. Burschka, N. Pellet, S.-J. Moon, R. Humphry-Baker, P. Gao, M. K. Nazeeruddin, M. Graetzel, *Nature* **2013**, 499, 316.

- [31] F. Liu, Q. Dong, M. K. Wong, A. B. Djuricic, A. Ng, Z. Ren, Q. Shen, C. Surya, W. K. Chan, J. Wang, A. M. C. Ng, C. Liao, H. Li, K. Shih, C. Wei, H. Su, J. Dai, *Adv. Energy Mater.* **2016**, *6*, 1502206.
- [32] N. Li, S. Tao, Y. Chen, X. Niu, C. K. Onwudinanti, C. Hu, Z. Qiu, Z. Xu, G. Zheng, L. Wang, *Nat. Energy* **2019**, *4*, 408.
- [33] Y. Wu, X. Li, S. Fu, L. Wan, J. Fang, *J. Mater. Chem. A* **2019**, *7*, 8078.
- [34] P. Zhu, S. Gu, X. Luo, Y. Gao, S. Li, J. Zhu, H. Tan, *Adv. Energy Mater.* **2020**, *10*, 1903083.
- [35] C. Wang, J. Wu, S. Wang, X. Liu, X. Wang, Z. Yan, L. Chen, X. Liu, G. Li, W. Sun, Z. Lan, *ACS Appl. Mater. Interfaces* **2021**, *13*, 50083.
- [36] C. Liu, L. Zhang, Y. Li, X. Zhou, S. She, X. Wang, Y. Tian, A. K. Y. Jen, B. Xu, *Adv. Funct. Mater.* **2020**, *30*, 1908462.
- [37] J.-F. Liao, W.-Q. Wu, J.-X. Zhong, Y. Jiang, L. Wang, D.-B. Kuang, *J. Mater. Chem. A* **2019**, *7*, 9025.
- [38] S. Y. Park, K. Zhu, *Adv. Mater.* **2022**, <https://doi.org/10.1002/adma.202110438>.
- [39] Z. Liu, K. Deng, J. Hu, L. Li, *Angew. Chem., Int. Ed.* **2019**, *58*, 11497.